Impact of post-rainfall evaporation from porous roof tiles on building cooling load in subtropical China

Lei Zhang[1*], Rongpeng Zhang[2], Tianzhen Hong[2], Yu Zhang[3], Qinglin Meng[1]
[1]School of Architecture, State Key Lab of Subtropical Building Science, South China University of Technology, Guangzhou, Guangdong 510641, China
[2]Building Technology and Urban Systems Division, Lawrence Berkeley National Laboratory, Berkeley, CA 94720, USA
[3]School of Chemistry and Chemical Engineering, South China University of Technology, Guangzhou, Guangdong 510641, China
*Corresponding author: Lei Zhang. Telephone/fax number: 862087110164, E-mail address: arzhang@scut.edu.cn.

Abstract:
Rainfall occurs frequently in subtropical regions of China, with the subsequent water evaporation from building roofs impacting the thermal performance and the energy consumption of buildings. We proposed a novel simulation method using actual meteorological data to evaluate the impact of post-rainfall evaporation from porous roof tiles on building cooling load. New features were developed in EnegryPlus to enable the simulation: (1) an evaporation latent heat flux source term was added to the heat balance equation of the external surface, and (2) algorithms for the evaporative cooling module (ECM) were developed and implemented into EnergyPlus using the EnergyPlus Runtime Language (Erl). The ECM was validated using experimental data and there was good agreement between the simulated and experimental result. Then the ECM was used to assess the impact of evaporation from porous roof tiles on the cooling load of a one-floor building in subtropical China. The results show that the evaporation process decreased the maximal values of the external and internal roof surface temperatures by up to 6.4 ℃ and 3.2 ℃, respectively, while the lower internal surface temperature decreased the room accumulated cooling load by up to 14.8% during the hot summer period. The enhanced EnergyPlus capability can be used to evaluate the evaporative cooling performance of roofs with water-storage mediums, as well as to quantify their impact on building cooling loads.

Keywords:
Rainfall event; Evaporative cooling; EnergyPlus; Building energy simulation; Cooling load; Subtropical China

1. Introduction

The subtropical areas of China are characterized by a monsoon climate, with the precipitation between May and October accounting for approximately 85% of the annual precipitation [1]. In addition, this period of frequent rainfall coincides with that of high temperatures [2]. This climatic feature facilitates evaporative cooling through the phase change of rainwater received in porous building materials and other specially designed structures. The consequence is a significant reduction of the external surface temperature of building envelopes [3-5], decreased heat flow into buildings [6-8], and lower cooling energy demands [9-11]. However, existing building energy simulation platforms such as EnergyPlus do not consider this evaporative cooling effect in heat gain calculations for building envelopes in areas of frequent rainfall [12].

Although several studies have been conducted to investigate the effect of rainfall on building envelopes, they mainly focused on moisture content and transport, and their effects on the building's performance and durability [13-15]. Moreover, most of the pioneering studies in the field were conducted in cold or temperate areas, where the buildings are exposed to alternating cold and hot seasons, and the combination of rainfall loads and cold temperatures constitute a huge challenge to building materials and construction systems [16-18]. It is obvious that this condition is dissimilar for subtropical areas; therefore, there should be differences in the approach to rainfall and buildings. An example of this difference is that buildings in subtropical areas can benefit from the evaporative cooling effect of frequent rainfall.

There is limited research on the positive effects of rainfall on the thermal performance of buildings in subtropical areas. Rao investigated the effect of intermittent rainfall on the energy performance of a building in Singapore [11]. Rainfall was simulated in the experiment by spraying water over a plastered brick wall on a bright sunny day, and the evaporative cooling effect of water was investigated to reduce the energy consumption of the test room by up to 25%. Using a similar rainfall simulation method, Zhang et al. [10] comparatively analyzed the energy saving afforded by an evaporative cooling wall externally decorated with porous tiles in the Chinese city of Guangzhou. Two rooms with the same construction features, orientation, and dimensions were compared, and the air conditioning power consumption was found to have decreased by 35.29–68.27% in the room where the simulated rainfall was carried out. Jayamaha et al. [19, 20] demonstrated a method to account for rainfall effects on the heat gain of a wall using the DOE-2 building energy estimation software as reference. Specifically, the authors adjusted the heat transfer coefficient to account for the surface heat loss due to the rainfall effect on the heat flux through the wall surface. In addition, to account for the post-rainfall drying effects of using porous building walls in the software, the modified sol-air temperature was used instead of the dry-bulb temperature and solar radiation intensity in the DOE-2 weather file. However, in calculating the modified sol-air temperature, the authors ignored the effects of outdoor conditions such as the prevailing solar radiation and wind speed on the drying rate (i.e., evaporation rate). In addition, the study only utilized isolated walls and discrete “characteristics days” to represent an entire year in the simulations [11]. The most recent study on this topic was conducted by Diaz and Osmond [11] focusing on parametric investigation based on the rainfall intensity. They performed whole-building simulations in WUFI Plus to estimate the hygrothermal performances of small buildings at wet, wet-dry, and dry tropical locations, respectively. Their results showed that rainfall significantly affects the cooling performance of a building. When the effect of rainfall was neglected, the outward total heat transfer per unit area from all the outdoor surfaces was

overestimated by 20% for a rainy month, and by 10% for the entire year; the corresponding values for the indoor wall surfaces were 7% and 5%, respectively. The maximum temperature reductions due to rainfall was determined to be 7.4 ℃ for outdoor surfaces, 1 ℃ for indoor surfaces, 0.4 ℃ for indoor air temperature, and 0.5 ℃ for indoor operative temperature. However, the hourly climate data used for the simulation was generated from the monthly data using Meteonorm software, and thus, was not representative of the actual weather conditions.

To summarize, although rainfall occurrences and the subsequent evaporation processes are noteworthy features of subtropical areas, and their effects on thermal and energy performances of buildings are significant, limited progress has been made on this topic in the last two decades, and many aspects of the effects still need to be explored. Specifically, the observed gaps in the literature include: (1) the thermophysical parameters of some water-storage mediums remain uncertain, (2) lack of integration of the evaporative cooling module with dynamic building energy simulation programs, and (3) the effect of post-rainfall evaporation on the cooling load of a building under actual weather conditions has not been well analyzed. To address the aforementioned gaps, this study made new contributions including: (1) the thermophysical parameters of a water-storage medium (i.e., a widely used porous tile) were investigated, (2) EnergyPlus Runtime Language (Erl) was used to develop an evaporative cooling module, which was integrated into the EnergyPlus code using the Energy Management System (EMS) feature, and (3) the actual meteorological data for Guangzhou from April 1 to August 30, 2012 was employed as the weather file in the EnergyPlus simulations.

The rest of this article is organized as follows. Section 2 describes the material and methodology. Section 3 describes the validation results of the ECM. Section 4 presents the effect of evaporation from porous roof tiles on building cooling load. Finally, the main conclusions drawn from the study are presented in Section 5.

2. Methodology and Material Properties Tests

The overall research roadmap is organized as follows. Firstly, we test the corresponding thermophysical parameters of the water-storage medium, including thermal conductivity, specific heat capacity, solar and thermal absorptances, which are important for the heat transfer process calculation. Then we develop the evaporative cooling module and integrate it into the heat balance equation of the external surface in EnergyPlus as an evaporation latent heat flux source term. Subsequently, in order to validate the accuracy of the evaporative cooling module in EnergyPlus, the simulated internal and external surface temperatures as well as internal surface heat flux of the roof considering the evaporation process were compared with the experimental results reported in literature. At the end, a box-shaped room with a south-facing window and the actual meteorological data were used to evaluate the evaporative cooling performance of roofs with water-storage mediums.

2.1 Water-storage medium

A porous tile was selected as the water-storage medium for the present study because it is commonly used to decorate the exterior surface of building envelopes (roofs and walls), and its evaporative cooling performance has also been previously demonstrated [10, 21, 22]. The considered tile was 240 mm long, 50 mm wide, and 10 mm thick, and had a mass saturated water content of 11.80% [23].

Building energy simulation requires the thermophysical properties of the building materials as

fundamental inputs, including the thermal conductivity, specific heat capacity, and solar and thermal absorptances. Although the thermophysical properties of the commonly used building materials have been reported in several works, those of porous tiles remain uncertain. The following processes were used to measure the thermophysical properties of the porous tiles used in this study.

(1) The dry porous tiles were ground into powder and the thermal conductivity and specific heat capacity of the powder were measured using a dual needle probe system, which is a modification of the transient line heat source described in IEEE 442-1981 [24] and ASTM D5334 [25]. The measurements were specifically carried out using a KD2 Pro analyzer with a 30-mm-long SH-1 dual needle probe produced by Decagon Devices. The dual-needle probe comprises a heater needle and a temperature sensor needle separated by a distance of 6 mm. Hence, by determining the travel time of heat pulse and the resultant temperature change, the thermal conductivity and specific heat capacity of the examined material can be evaluated. The thermal conductivity and specific heat capacity of the porous tiles determined by this method were 0.2 W/m·K and 740 J/kg·K, respectively. Considering the thinness of the porous tiles (thickness of 10 mm), the effects of changes in the thermal conductivity and specific heat capacity due to varying water content on the thermal performance of the roof can be neglected.

(2) A spectrophotometer and a portable emissometer were used to measure the solar and thermal absorptances of the porous tiles for different water contents. Three specimens were prepared from the same batch of porous tiles. The specimens were dried in an oven at 110±5 °C until a constant weight was attained, after which they were stored under the test conditions (temperature of 24±0.3 °C and relative humidity of 45±2%) until their masses stabilized to within 0.1%. The three specimens were then immersed in a water tank at the same time and left to soak for 24 h. They were subsequently stored again under the test conditions to attain different water contents. The solar and thermal absorptances of the specimens were measured in accordance with ASTM E903 [26] and ASTM C1371 [27], respectively. The results are shown in Fig. 1. As can be observed from Fig. 1(a), the solar absorptance increases gradually with increasing water content. This is due to the decreasing relative refractive index of the medium and the resultant scattering of light in the direction of the incident radiation, with higher absorption of incident photons [28]. A linear relationship between the solar absorptance and the mass water content was extracted from Fig 1(a), as expressed by equation (1).

$$\alpha_s = 0.667 \cdot w_c + 74.182 \tag{1}$$

The term mass water content (w_c) is defined as the ratio of the mass of water in the specimen to the mass of the dry specimen, as described in equation (2).

$$w_c = \frac{m_{wet} - m_{dry}}{m_{dry}} \tag{2}$$

In the simulation of the building energy, equation (1) was used to estimate the surface solar absorptance under different mass water contents.

It can be observed from Fig. 1(b) that the impact of the mass water content on thermal absorptance is not as significant as its impact on solar absorptance. Specifically, the mean value of the thermal absorptance is 0.83 if the specimen is dry, while the thermal absorptance fluctuates

between 0.88 and 0.94 if the specimen is wet. Therefore, the thermal absorptance was set to the average value of 0.89 during the simulation process.

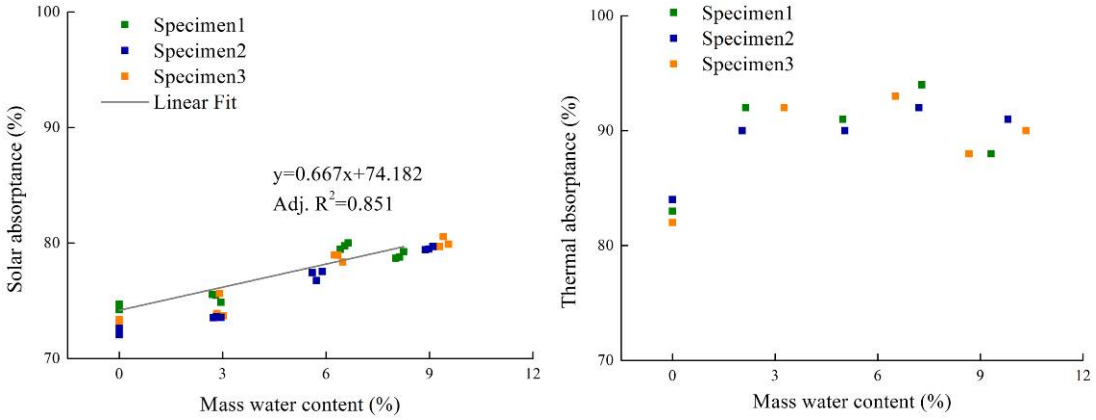

(a) Solar absorptance vs. water content (b) Thermal absorptance vs. water content

Fig. 1 Solar and thermal absorptances of the porous tiles with respect to the mass water content

2.2 Evaporative cooling module

The moisture balance at an external surface is made up of precipitation and vapor exchange, while the heat balance comprises solar and thermal radiation, convective heat exchange, sensible heat transfer due to precipitation, and latent and sensible heat transfer due to vapor exchange [29]:

$$q = \left(q_s + q_t + q_c + q_p + q_e\right) \cdot \mathrm{n} \tag{3}$$

$$g = \left(g_p + g_e\right) \cdot \mathrm{n} \tag{4}$$

The boundary flow terms are assumed positive when the mass or energy content of the simulated construction increases.

The method for calculating the first three terms on the left side of equation (3) is described in an EnergyPlus reference work [12]. Equations (5) and (6) are respectively used to calculate q_p [30] and q_e [23].

$$q_p = g_p c_w \left(t_p - t_s\right) \tag{5}$$

$$q_e = g_e \cdot \left(2491.146 - 2.302 \cdot t_a\right) \tag{6}$$

Evaporation from the porous tiles is mainly by vapor movement from a high vapor pressure region to a low vapor pressure region [31]. An analysis of the process involves a mathematically rigorous and complex convergence procedure, which makes the calculation of the evaporation rate complex [21]. To address this issue, based on the measured evaporation rate, Zhang et al. developed a multivariate nonlinear model for predicting the evaporation rate of the porous tile [21]. The model, which is presented as equation (7), was used in the present study to calculate the evaporation rate and the corresponding latent heat transfer from the porous tiles.

$$g_e = 0.000842 \cdot q_s + e^{1.45 - \frac{77.2}{t_a - 14.4}} + e^{1.3 \cdot r_h - 0.01 \cdot (r_h)^2 - 45.6} + e^{-1.2 - \frac{7.24}{w_v + 0.355}} - 0.00399 \tag{7}$$

Equation (8) was used to convert the precipitation from mm to g.

$$g_p = p \times 1 \times 1000 \tag{8}$$

2.3 Integration with EnergyPlus

The open source simulation program EnergyPlus was used to simulate the effect of evaporation from porous tiles on the building cooling load. The program calculates the cooling load required to maintain the thermal control setpoints based on the user's description of the building, including its physical properties and the utilized mechanical systems [32-34]. The EnergyPlus source code was updated in this study to add the evaporation latent heat flux source term to the heat balance equation of the external surface, to facilitate the simulation of the effect of evaporative cooling from the external porous layer of the building on energy consumption.

Energy Management System (EMS) is an advanced feature of the EnergyPlus software, which enables the development of custom control and modeling routines. An essential part of the EMS module is the EnergyPlus Runtime Language (Erl), which is a simple programming language for specifying the EMS control algorithms. The EMS and Erl facilitate the use of the software to simulate many novel control strategies that were not possible with previous generations of building energy simulation programs [35]. In this study, Erl was used to develop the evaporative cooling module of the porous tiles, and the module was then integrated into EnergyPlus through the EMS. Equation (7) was used to calculate the latent heat flux at each time step based on the mass water content and EnergyPlus weather data. The EMS actuator could be used to override the calculated external heat flux into the model building, thus facilitating the investigation of the effects of the evaporation process on the surface temperature of the roof with porous tiles, as well as the corresponding cooling load.

3. Validation of the ECM

To validate the accuracy of the ECM in EnergyPlus, the simulated internal and external surface temperatures as well as the internal surface heat flux of the roof considering the evaporation process were compared with the experimental results reported by Zhang et al. [23].

The experiment was modeled in EnergyPlus with appropriate building materials, thermal properties and configurations. The roof was modeled using the ECM proposed in this study considering the evaporation process. The environmental parameters in the experimental study were employed as the weather boundary conditions of EnergyPlus. The simulation run period was consistent with the experiment duration. The external and internal surface temperatures as well as the internal surface heat flux of the roof considering the evaporation process were used for the validation. Details of the validation setup are provided in Appendix A.

Two common error indexes, the mean bias error (MBE) and the cumulative variation of root mean square error (CVRMSE), were used to evaluate the computational accuracy of the ECM in EnergyPlus. The MBE and CVRMSE were calculated using equations (9) and (10), respectively [36-37]:

$$\mathrm{MBE} = \frac{\sum_{i=1}^{j} \left(VA_{m,i} - VA_{s,i} \right)}{\sum_{i=1}^{j} VA_{m,i}} \tag{9}$$

$$\mathrm{CVRMSE} = \frac{\sqrt{\dfrac{\sum_{i=1}^{j}\left(VA_{m,i} - VA_{s,i}\right)^2}{j}}}{\left(\dfrac{\sum_{i=1}^{j} VA_{m,i}}{j}\right)} \tag{10}$$

Fig. 2 shows the 96-h variations in the measured and simulated values. The MBEs of the external and internal surface temperatures as well as internal surface heat flux were 3.0%, 0.1%, and 3.3%, respectively. The CVRMSEs of the external and internal surface temperatures as well as internal surface heat flux were 3.4%, 2.0%, and 8.7%, respectively.

The discrepancy may arise from the experimental error, as well as the difference between the actual and the adopted values of material properties or the overall heat transfer coefficients. However, the accuracy at this level is sufficient to characterize the temperature and heat flux variations resulted from evaporation process of porous roof tiles.

That is, the proposed module yielded sufficient accurate results in quantifying the cooling effect due to the evaporation process. The validated ECM was then used to investigate the effect of post-rainfall evaporation from porous roof tiles on the building cooling load.

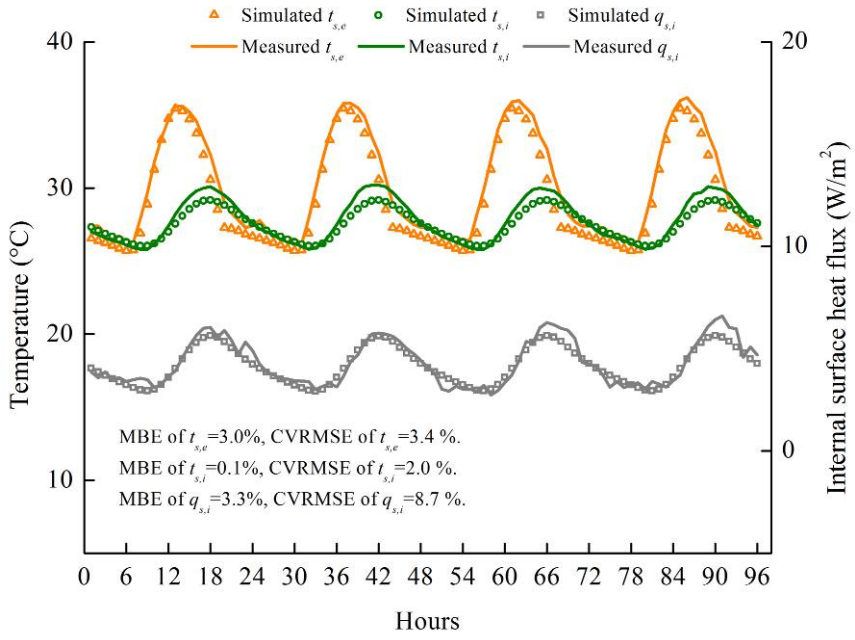

$t_{s,e}$, $t_{s,i}$, and $q_{s,i}$ are external surface temperature, internal surface temperature, and internal surface heat flux, respectively.

Fig. 2 Variations of the measured and the simulated surface temperatures as well as heat flux

4. Effect of evaporation on building cooling load

4.1 Building model and simulation parameters

The purpose of the present study is to provide a calculation method to evaluate the impact of post-rainfall evaporation from porous roof tiles on building cooling load rather than analyze the energy efficiency potential of evaporative cooling from porous tiles of an actual building. Based on this purpose, a box-shaped room with a south-facing window was used to develop the building model for the EnergyPlus simulation, as shown in Fig. 3. This building model simplifies the

impact of the building geometry, internal gains, HVAC systems, and others on the calculation results. The building materials and their thermophysical parameters are summarized in Table 1, while the EnergyPlus energy simulation settings are presented in Table 2.

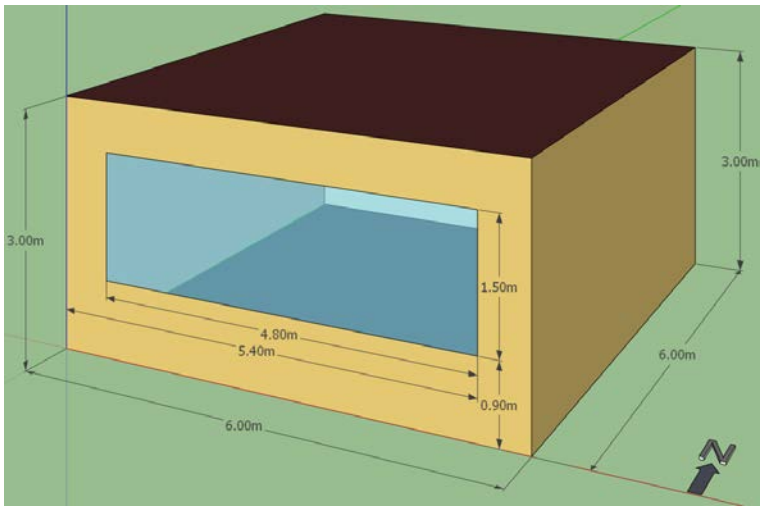

Fig. 3 Building model for EnergyPlus simulation

The effectiveness of passive building energy efficiency technologies is related to the U-value of the building envelope. Hence, three types of roofs were considered in this study, namely, an un-insulated roof (UIR), a moderately insulated roof (MIR), and a well-insulated roof (WIR) (see Fig. 4). The evaporative cooling potentials of all three roof types were examined.

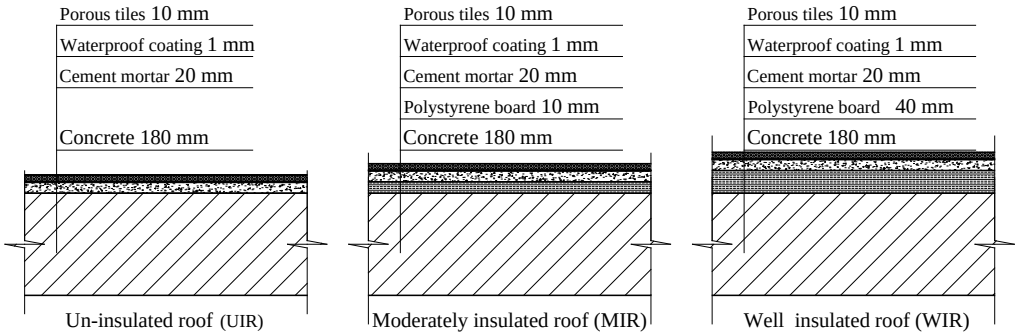

Fig. 4 Three types of roofs investigated in this study

Table 1 Building materials and their thermophysical parameters

Building part	Material (from outside to inside)	Thickness d (mm)	Thermal conductivity λ (W/m·K)	Density ρ (kg/m^3)	Specific heat c (kJ/kg·K)
Roof	Porous tile	10	0.20	1540	0.74
	Waterproof coating*	-	-	-	-
	Cement mortar	10	0.97	1600	0.90
	Polystyrene board	0,10,40	0.033	32	1.21
	Concrete	180	1.40	1920	0.90
Wall	Waterproof coating*	-	-	-	-
	Cement mortar	20	0.97	1600	0.90
	Aerated concrete brick	200	0.22	700	1.05

	Cement mortar	20	0.97	1600	0.90
Floor	Adiabatic floor	-	-	-	-

* The waterproof coating was very thin, thus, its thermal resistance was ignored.

Table 2 EnergyPlus simulation settings

Object	Description
EnergyPlus version	8.1
Inside surface convection algorithm	TARP
Outside surface convection algorithm	DOE-2
Heat balance algorithm	Conduction transfer function
Zone air heat balance algorithm	Third-order backward difference
Numbers of timesteps per hour	60
Run period	April 1 to August 30, 2012
Window	U-factor = 6.0 W/m^2·K Solar heat gain coefficient = 0.8
Internal Gains	None
Zone HVAC	Ideal load air system
Cooling setpoint temperature	Always 26 °C

4.2 Meteorological data

In the present study, the Guangzhou meteorological data from April 1 to August 30, 2012 was used as the weather file for EnergyPlus. It can be observed from the data shown in Fig. 5 that rainfall events occurred frequently in Guangzhou during the analysis period, with the total precipitation being 1294.8 mm. Rainfall events particularly occurred during the hot summer period from June to August, which accounted for a precipitation of 624.0 mm. This provided sufficient water resources for the occurrence of evaporation from the porous tiles. Solar energy resources are also abundant in Guangzhou. The total energy during the analysis period was 2259 MJ/m^2, which afforded adequate conditions for the continual evaporation of water from the porous tiles. Moreover, although the relative humidity in the city is high, which is not conducive to evaporation, the supplementary effect of the wind speed facilitated dynamic evaporation due to the water vapor pressure difference, accounting for 20% of the total evaporation [23]. Thus, the prevailing conditions during the considered hot summer period in Guangzhou facilitated the evaporation of water stored in the porous roof tiles, with the resultant cooling effect on the building.

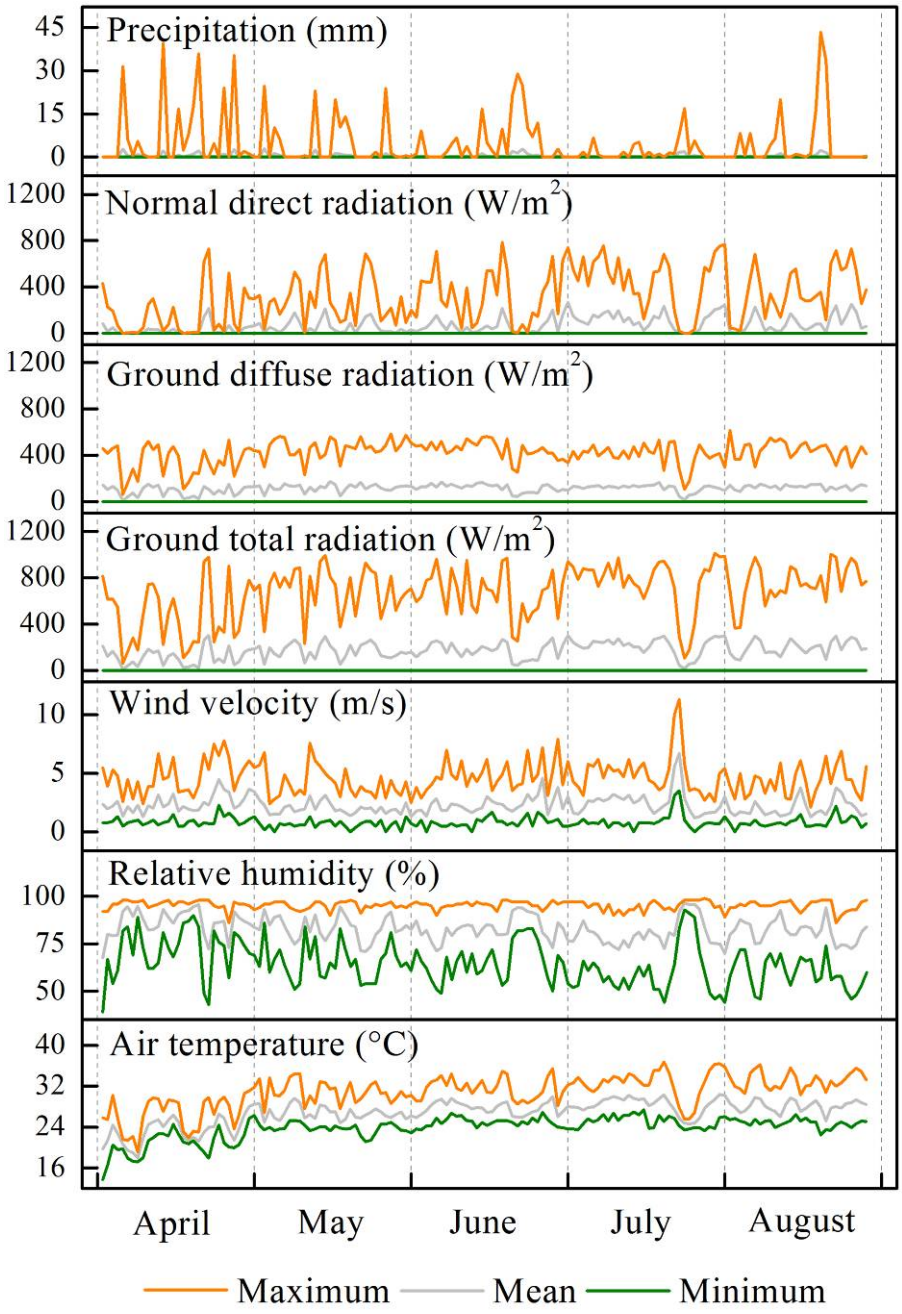

Fig. 5 Guangzhou meteorological data from April 1 to August 30, 2012

4.3 Temporal variations of moisture in the porous tiles

The temporal variations of the precipitation, mass water content, and evaporation rate are shown in Fig. 6.

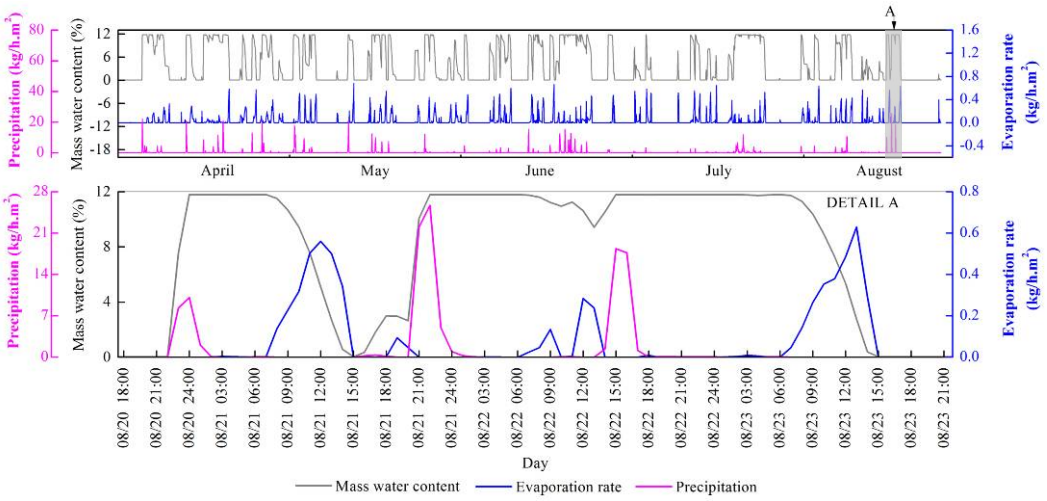

Fig. 6 Temporal variations of the precipitation, mass water content, and evaporation rate.

When it rained, the porous tiles on the roof absorbed rainwater, resulting in an increased water content. The saturated mass water content of the tiles was 11.8%, which implies that the maximum water that they could absorb per 1 m^2 was approximately 1.8 kg. The additional rainwater flowed away as runoff. After a rainfall event, the evaporation process commenced, with a decrease in the water content of the tiles (evaporation was ignored during the rainfall owing to the nearly 100% relative humidity of air). The cumulative amount of evaporation during the summer period was 83.6 kg/m^2, which is approximately 13.4% of the total precipitation over the three-month period.

Taking the results for 18:00 August 20 to 21:00 August 23 as an example, three heavy rainfall events occurred during the period, each lasted until midnight, resulting in the saturation of the porous tiles. Due to the low water vapor pressure difference between the air and the surface of the porous tiles, evaporation during the nighttime was not significant. The evaporation rate always peaked during periods of high solar radiation intensity and high air temperature. The highest hourly evaporation rate during the period in focus was 0.63 kg/m^2, which specifically occurred at 13:00 August 23 when the total solar radiation was 1006 W/m^2 and the air temperature was 32.0 °C.

4.4 Surface heat flux and temperature

The results from August 20 to 26 are representative of the results obtained from April to August because rainfall and evaporation process alternately occurred during these seven days. Specifically, intermittent rainfall was observed on the first four days (August 20 to 23) resulting in high water content in the tiles, especially on August 23 when the water content in the tiles was close to the saturated water content, which produced significant evaporative cooling effect. As for the later three days (August 24 to 26), the evaporative cooling effect was weakened due to the low water content in the tiles. Therefore, we selected the data during these seven days to plot Figs. 7 and 8 and the data on August 23 to analyze the evaporative cooling effect in detail.

Figure 7 shows the temporal variation of the heat flux on the external surface of the roof, taking evaporation into consideration. The sum of q_s, q_t, q_c, q_d, q_e, and q_p is zero (negligible non-zero values are due to computational errors), which implies that the external surface of the roof is in a heat balance state. It can also be observed that in the daytime, the latent heat transfer q_e is the main heat dissipation route from the external surface of the roof, accounting for a large

proportion of the net shortwave radiation, which reduced the external surface temperature and the corresponding internal surface temperature, as shown in Fig. 8.

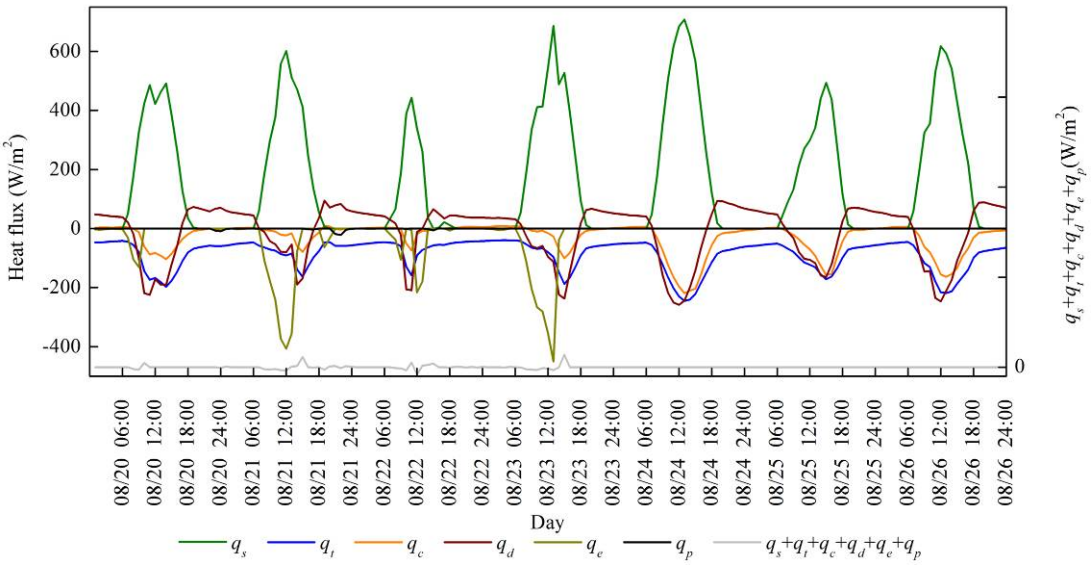

Fig. 7 Temporal variation of the heat flux on the external surface of the roof, taking evaporation into consideration

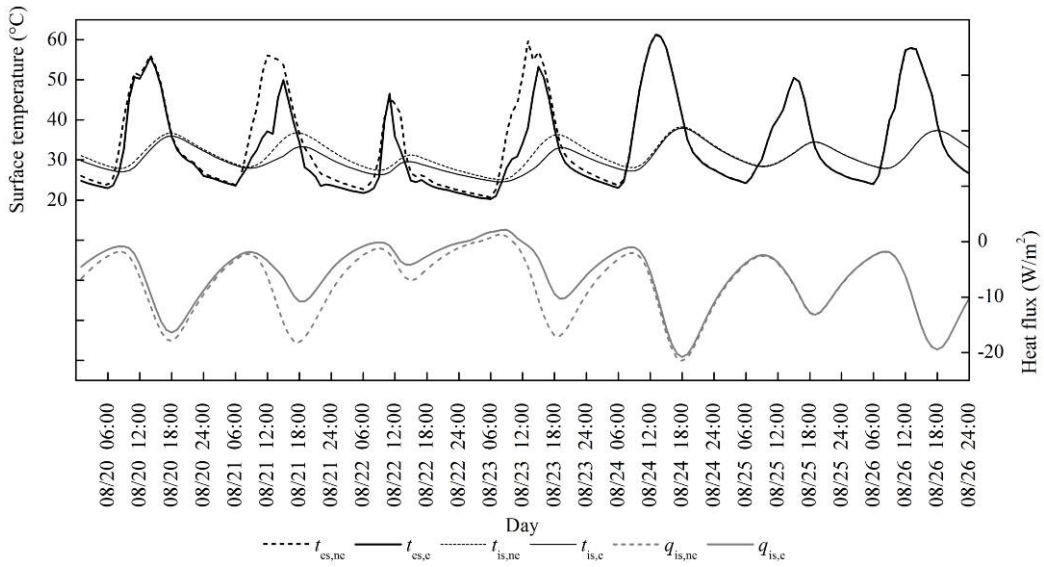

$t_{es,ne}$: external surface temperature of non-evaporation roof. $t_{es,e}$: external surface temperature of evaporation roof. $t_{is,ne}$: internal surface temperature of non-evaporation roof. $t_{is,e}$: internal surface temperature of evaporation roof. $q_{is,ne}$: internal surface heat flux of non-evaporation roof. $q_{is,e}$: internal surface heat flux of evaporation roof.

Fig. 8 Temporal variation of the surface temperature and heat flux on the roof, taking evaporation into consideration

Taking the simulation results for August 23 as an example, after three days of intermittent rainfall, the porous tiles on the roof were close to saturation. Beginning from 7:00, the evaporation rate significantly increased, resulting in increased latent heat transfer. At 13:00, the latent heat transfer peaked at 450.4 W/m^2, using up 65.6% of the surface net solar radiation. At the same time, the conduction heat flux into the roof was 60.3% lower than that when evaporation was not

considered.

In the morning (7:00 AM–12:00 noon), the external surface temperatures of both the evaporation and non-evaporation roofs increased, although the growth of the former was significantly lower. The maximum external surface temperature of the non-evaporation roof was 59.7 °C, which occurred at 13:00, at which time the external surface temperature of the evaporation roof was 38.0 °C. However, the subsequent significant decrease in the water content of the evaporation roof caused a sharp increase in the roof external surface temperature, which reached a peak value of 53.3 °C at 15:00. When the water content decreased to the residual value, the evaporation process ceased. At this time, the external surface temperature of the evaporation roof was close to that of the non-evaporation roof. Regarding the internal surface temperature, the variations for the evaporation and non-evaporation roofs were similar to those of the corresponding external surfaces, with the internal surface temperature of the evaporation roof lower than that of the non-evaporation roof. However, there was an attenuation of the amplitudes of the internal surface temperatures for both cases, as well as phase delay of the temperature wave due to the effect of heat storage in the roof. The peak internal surface temperatures of the evaporation and non-evaporation roofs were 33.1 °C and 36.3 °C, respectively, which occurred at 19:00. Further, during the analyzed seven days, the heat transfer from the internal surface of the evaporation roof was 21.2% lower than that from the internal surface of the non-evaporation roof.

4.5 Cooling load saving potential

The temporal variations of the room cooling loads between August 20 and August 26 are shown in Fig. 9. Evaporation from the porous tiles of the evaporation roof significantly decreased the cooling loads of the room owing to the reduced heat transfer from the internal surface of the roof to the room space. The simulation results for the seven-day duration show that the accumulated cooling load of the room with the evaporation roof was 151.5 kWh, which is 15.3% lower than that of the room with the non-evaporation roof.

Additionally, the cooling load of the room without considering the roof evaporation process minus the cooling load of the room considering the roof evaporation process was defined as the cooling load reduction value.

Two peak values of the cooling load reduction could be observed in Fig. 9. One occurred on 17:00 August 21, five hours later than the occurrence of the maximum value of the evaporation rate, which is 0.56 kg/m^2. At 17:00 August 21 the cooling load reduction is 560.8 Wh. The other occurred at 17:00 August 23, four hours later than the occurrence of the maximum value of the evaporation rate, which is 0.63 kg/m^2. At 17:00 August 23 the cooling load reduction is 577.9 Wh. It indicated that the peak value of evaporation rate usually occurs at periods with intense solar radiation, while the peak value of cooling load reduction could be lagged for a period of time depending on the thermophysical parameters of the building envelope.

From August 24 to 26, because of the absence of precipitation and the consequent evaporative cooling of porous roof tiles, the difference of the cooling load between rooms with and without considering roof evaporation process was decreasing, and eventually disappeared.

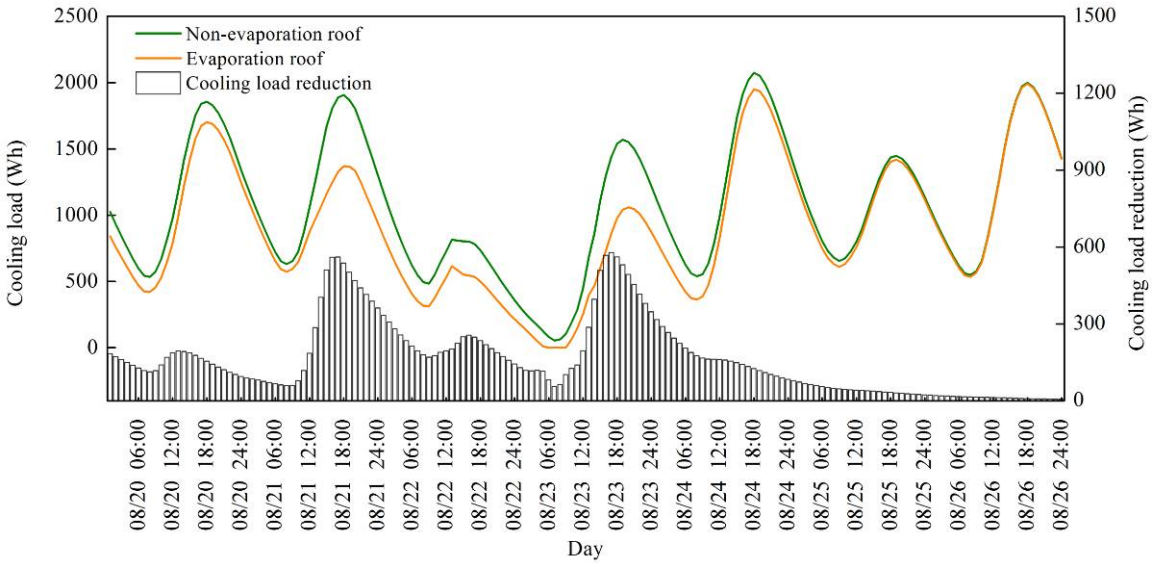

Fig. 9 Temporal variations of the cooling loads of the non-evaporation and evaporation roofs.

The absolute and relative values of the cooling load saving potentials are defined by equations (11) and (12), respectively.

$$S_{a,c} = C_n - C_e \tag{11}$$

$$S_{r,c} = \frac{C_n - C_e}{C_n} \cdot 100\% \tag{12}$$

To investigate the effect of the U-value of the roof structure on the effectiveness of the evaporative cooling technology, the cooling load saving potentials of the three considered types of roofs (UIR, MIR, and WIR) were calculated using equations (11) and (12), respectively. The results are presented in Table 3.

Table 3 Cooling load saving potentials

Month	Cooling load saving potentials						Precipitation (mm)
	UIR		MIR		WIR		
	A. V. * (kWh)	R. V. * (%)	A. V. (kWh)	R. V. (%)	A. V. (kWh)	R. V. (%)	
May	107.4	20.2	61.5	15.0	28.0	8.3	300.8
June	115.2	20.4	66.7	15.2	30.4	8.3	302.8
July	92.4	12.2	52.4	9.1	23.3	5.1	138.7
August	94.3	11.9	52.7	8.6	23.6	4.7	182.5

*A. V.=Absolute value, R. V.=Relative Value.

It can be observed in Table 3 that the cooling load saving potentials decreased with the enhancement of the roof insulation performance because of the declined inward flux. Based on the results for July, the cooling load saving potentials of the present UIR, MIR, and WIR were 92.4 kWh (12.2%), 52.4 kWh (9.1%), and 23.3 kWh (5.1%), respectively.

The close relationship between the cooling load saving potential and the amount of precipitation can also be observed in Table 3. With increasing monthly precipitation, the water-storage medium on the roof captures more water for evaporative cooling, with a resultant increase in the cooling load saving potential. Taking the results for June and July as examples, the precipitation in June

was 2.2 times that in July, while the absolute values of the cooling loads saving potentials of UIR, MIR, and WIR in June were approximately 1.3 times those in July.

It is noted that the cooling load saving potentials of July and August were very close to each other, although the monthly precipitation in August was 43.8 mm higher than that in July; this indicates that besides the amount of precipitation, other meteorological factors (such as temperature, solar radiation, wind velocity, humidity, and temporal pattern of precipitation) could also influence the water absorption as well as subsequent evaporation process, and in turn, the cooling load saving potentials. This issue is beyond the scope of the present study and requires further investigations.

5. Conclusions

In the present study, an evaporative cooling module (ECM) was developed and integrated into EnergyPlus. The integrated ECM was validated against reported experimental data and there was good agreement between the simulated results and the measured results.

The effects of evaporation from porous roof tiles on building cooling load were analyzed using the integrated ECM. The results show that buildings in subtropical areas can benefit from the evaporative cooling effect of frequent rainfall. Specifically, the evaporation process decreased the maximal external and internal roof surface temperatures by up to 6.4 °C and 3.2 °C, respectively, and the lower internal surface temperature reduced the room accumulated cooling load by up to 14.8% during the hot summer period (from June to August).

On the other hand, the analysis also revealed that if the evaporation process was ignored during the simulation procedure the accumulated cooling loads could be overestimated by 4.7–20.4% depending on the roof insulation condition and meteorological factors. Therefore, the effect of rainfall and the subsequent evaporation process are non-negligible in building energy simulation for subtropical areas, which are characterized by abundant precipitation.

The authors plan further study to investigate the water absorption and evaporation characteristics of different porous building materials to acquire comprehensive data for the assessment of the effect of evaporative cooling on building energy consumption. Additional research can also consider the optimization of rainfall water and spraying water to enhance the evaporative cooling effect by using the simulation methods proposed in the present study.

Acknowledgments

This work was supported by the National Natural Science Foundation of China (grant numbers 51678243, 51378210), Guangdong Natural Science Foundation (grant number 2016A030313506), Project of State Key Lab of Subtropical Building Science, South China University of Technology (grant number 2015ZC14 and 2018ZA01), and Fundamental Research Funds for Central Universities (grant numbers 2017ZD017 and 2017ZD039). This work was also supported by the Assistant Secretary for Energy Efficiency and Renewable Energy, the U.S. Department of Energy under Contract No. DE-AC02-05CH11231.

Appendix A.

The ECM was validated using a case study derived from the previously published work of Zhang et al. [23], who conducted wind tunnel measurements of the un-insulated roof construction mentioned in section 4 of this article. The thermophysical properties of the building materials in Table 1 were employed for the simulation. The configurations of EnergyPlus are presented in Table

A1. The environment parameters for one cycle (24 h) in the experimental study were employed as the weather boundary conditions of EnergyPlus, as shown in Fig. A1. The simulation run period was set to 4 days, which is compatible with the experiment duration.

Table A1 EnergyPlus simulation settings for the validation of ECM

Object	Description
EnergyPlus version	8.1
Inside surface convection algorithm	TARP
Outside surface convection algorithm	DOE-2
Heat balance algorithm	Conduction transfer function
Zone air heat balance algorithm	Third-order backward difference
Numbers of timesteps per hour	60
Run period	96 h
Internal Gains	None
Zone HVAC	Ideal load air system
Cooling setpoint temperature	Always 22 °C

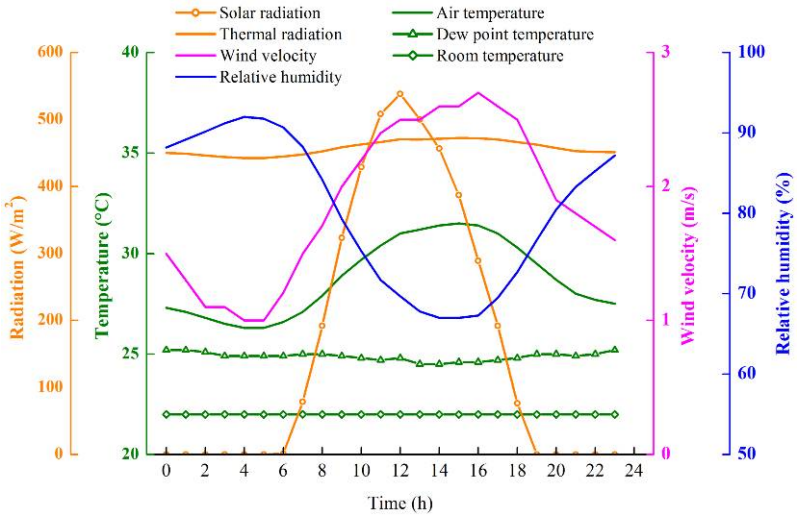

Fig. A1 Environmental parameters in the experimental study

Nomenclature

C_e: Accumulated cooling load of room considering evaporation from porous roof tiles (kWh)

C_n: Accumulated cooling load of room without considering evaporation from porous roof tiles (kWh)

c_w: Specific heat capacity of water (J/kg·°C)

g: Moisture flow (kg/m^2)

g_d: Weight of dry porous tiles (kg/m^2)

g_e: Evaporation rate (kg/m^2)

g_m : Weight of water in wet porous tiles (kg/m^2)

g_p : Amount of rainfall (kg/m^2)

j : Total number of measurement data points

m_{wet} : Mass of wet specimen (kg)

m_{dry} : Mass of dry specimen (kg)

n : A unit vector perpendicular to the construction's surface

p : Precipitation (mm)

q : Heat flow (W/m^2)

q_c : Convective flux exchange with outside air (W/m^2)

q_d : Conductive heat flux (W/m^2)

q_e : Latent heat transfer due to evaporation (W/m^2)

q_p : Sensible heat transfer due to precipitation (W/m^2)

q_s : Net short wavelength radiation heat flux on external surface (W/m^2)

q_t : Net long wavelength radiation flux exchange with air and surroundings (W/m^2)

r_h : Relative humidity (%)

$S_{a,c}$: Absolute cooling load saving potential (kWh)

$S_{r,c}$: Relative cooling load saving potential (%)

t_a : Air temperature (°C)

t_p : Precipitation temperature (°C)

t_s : Surface temperature (°C)

$VA_{m,i}$: i-th measured value

$VA_{s,i}$: i-th simulated value

w_c : Mass water content of wet porous tiles (%)

w_v : Wind velocity (m/s)

α_s : Solar absorptance (%)

References

[1] National Bureau of Statistics of China. China Statistical Yearbook, 2016.

[2] Q. Meng, Z. Wang, Y. Zhang, L. Zhao. Rainfall identification and estimation in Guangzhou area used for building energy simulation. Building and Environment, 42(8) (2007), pp. 3112-3122.

[3] S. Wanphen, K. Nagano. Experimental study of the performance of porous materials to moderate the roof surface temperature by its evaporative cooling effect. Building and Environment, 44(2) (2009), pp. 338-351.

[4] L. Pires, P.D. Silva, J.P. Castro Gomes. Performance of textile and building materials for a particular evaporative cooling purpose. Experimental Thermal and Fluid Science, 35(4) (2011), pp. 670-675.

[5] D. Karamanis, E. Kyritsi, S. Krimpalis. Well-ordered nanoporous materials for low-temperature water phase changes and solar evaporative cooling. Solar Energy Materials and Solar Cells, 139(2015), pp. 34-43.

[6] J. He, A. Hoyano. Experimental study of cooling effects of a passive evaporative cooling wall constructed of porous ceramics with high water soaking-up ability. Building and Environment, 45(2) (2010), pp. 461-472.

[7] W. Chen, S. Liu, J. Lin. Analysis on the passive evaporative cooling wall constructed of porous ceramic pipes with water sucking ability. Energy and Buildings, 86 (2015), pp. 541-549.

[8] Q. Meng, W. Hu. Roof cooling effect with humid porous medium. Energy and Buildings, 37(1) (2005), pp. 1-9.

[9] M. Santamouris, D. Kolokotsa. Passive cooling dissipation techniques for buildings and other structures: the state of the art. Energy and Buildings, 57 (2013), pp. 74-94.

[10] L. Zhang, X. Liu, Q. Meng, Y. Zhang. Experimental study on the impact of mass moisture content on the evaporative cooling effect of porous face brick. Energy Efficiency, 9(2) (2016), pp. 511-523.

[11] C.A. Diaz, P. Osmond. Influence of Rainfall on the thermal and energy performance of a low rise building in diverse locations of the hot humid tropics. Procedia Engineering, 180 (2017), pp. 393-402.

[12] US Department of Energy. EnergyPlus Documentation, 2013.

[13] D. Aelenei, F.M. Henriques. Analysis of the condensation risk on exterior surface of building envelopes. Energy and Buildings, 40(10) (2008), pp. 1866-1871.

[14] B. Blocken, J. Carmeliet. A simplified numerical model for rainwater runoff on building facades: possibilities and limitations. Building and Environment, 53 (2012), pp. 59-73.

[15] B. Blocken, D. Derome, J. Carmeliet. Rainwater runoff from building facades: a review. Building and Environment, 60 (2013), pp. 339-361.

[16] M. Abuku, H. Janssen, J. Poesen, S. Roels. Impact, absorption and evaporation of raindrops on building facades. Building and Environment, 44(1) (2009), pp. 113-124.

[17] V.M. Nik, S.O. Mundt-Petersen, A.S. Kalagasidis, P. De Wilde. Future moisture loads for building facades in Sweden: climate change and wind-driven rain. Building and Environment, 93 (2015), pp. 362-375.

[18] H. Ge, U.D. Nath, V. Chiu. Field measurements of wind-driven rain on mid-and high-rise buildings in three Canadian regions. Building and Environment, 116(2017), pp. 228-245.

[19] S.E.G. Jayamaha, S.K. Chou, N.E. Wijeysundera. Accounting for rain effects in building energy estimation. International Journal of Energy Research, 22(1) (1998), pp. 61-71.

[20] S.E.G. Jayamaha, N.E. Wijeysundera, S.K. Chou. Effect of rain on the heat gain through building walls in tropical climates. Building and Environment, 32(5) (1997), pp. 465-477.
[21] L. Zhang, R. Zhang, Y. Zhang, T. Hong, Q. Meng, Y. Feng. The impact of evaporation from porous tile on roof thermal performance: a case study of Guangzhou's climatic conditions. Energy and Buildings, 136 (2017), pp. 161-172.
[22] Y. Zhang, L. Zhang, Z. Pan, Q. Meng, Y. Feng, Y. Chen. Hydrological properties and solar evaporative cooling performance of porous clay tiles. Construction and Building Materials, 151 (2017), pp. 9-17.
[23] L. Zhang, Y. Feng, Q. Meng, Y. Zhang. Experimental study on the building evaporative cooling by using the climatic wind tunnel. Energy and Buildings, 104 (2015), pp. 360-368.
[24] IEEE, IEEE 442 guide for soil thermal resistivity measurements, in: Proceedings of the IEEE Standards Committee, Institute of Electrical and Electronics Engineers Inc., New York, 1981.
[25] ASTM, Standard Test Method for Determination of Thermal Conductivity of Soil and Soft Rock by Thermal Needle Probe Procedure, American Society for Testing and Materials, Philadelphia, 2000.
[26] E903-96: Standard test method for solar absorptance, reflectance, and transmittance of materials using integrating spheres, Annual Book of ASTM Standards, 1996.
[27] C1371-04a (2010) e1. Standard test method for determination of emittance of materials near room temperature using portable emissometers, American Society for Testing and Materials, West Conshohocken, PA, 2010.
[28] D.J. Sailor, D. Hutchinson, L. Bokovoy. Thermal property measurements for ecoroof soils common in the western US. Energy and Buildings, 40(7) (2008), pp. 1246-1251.
[29] H. Janssen, B. Blocken, J. Carmeliet. Conservative modelling of the moisture and heat transfer in building components under atmospheric excitation. International Journal of Heat and Mass Transfer, 50(5) (2007), pp. 1128-1140.
[30] G. Gan. Dynamic interactions between the ground heat exchanger and environments in earth-air tunnel ventilation of buildings. Energy and buildings, 85 (2014), pp. 12-22.
[31] F. Moukalled, N. Ghaddar, Y. Saleh, Z. Fawaz. Heat and mass transfer in moist soil, Part II. Application to predicting thermal signatures of buried landmines. Numerical Heat Transfer, Part B: Fundamentals, 49(5) (2006), pp. 487-512.
[32] C. Yan, S. Wang, K. Shan, Y. Lu. A simplified analytical model to evaluate the impact of radiant heat on building cooling load. Applied Thermal Engineering, 77 (2015), pp. 30-41.
[33] P.G. Loutzenhiser, H. Manz, C. Felsmann, P.A. Strachan, G. M. Maxwell. An empirical validation of modeling solar gain through a glazing unit with external and internal shading screens. Applied Thermal Engineering, 27(2) (2007), pp. 528-538.
[34] G. Barrios, J. Rojas, G. Huelsz, R. Tovar, S. Jalife. Implementation of the equivalent-homogeneous-layers-set method in whole-building simulations: Experimental validation. Applied Thermal Engineering, 125 (2017), pp. 35-40.
[35] K.K.C. Dahanayake, C.L. Chow. Studying the potential of energy saving through vertical greenery systems: Using EnergyPlus simulation program. Energy and Buildings, 138 (2017), pp. 47-59.
[36] M. Royapoor, T. Roskilly. Building model calibration using energy and environmental data. Energy and Buildings, 94 (2015), pp. 109-120.
[37] Tong, S., Li, H., Zingre, K.T., Wan, M.P., Chang, V.W.C., Wong, S.K., Toh, W.B.T. and Lee,

I.Y.L. Thermal performance of concrete-based roofs in tropical climate. Energy and Buildings, 76(2014), pp.392-401.